Can adding oil control domain formation in binary amphiphile bilayers?

Martin J. Greenall *[ab] **and Carlos M. Marques** [a]

Received Xth XXXXXXXXXX 20XX, Accepted Xth XXXXXXXXX 20XX
First published on the web Xth XXXXXXXXXX 200X
DOI: 10.1039/b000000x

Bilayers formed of two species of amphiphile of different chain lengths may segregate into thinner and thicker domains composed predominantly of the respective species. Using a coarse-grained mean-field model, we investigate how mixing oil with the amphiphiles affects the structure and thickness of the bilayer at and on either side of the boundary between two neighbouring domains. In particular, we find that oil molecules whose chain length is close to that of the shorter amphiphiles segregate to the thicker domain. This smooths the surface of the hydrophobic bilayer core on this side of the boundary, reducing its area and curvature and their associated free-energy penalties. The smoothing effect is weaker for oil molecules that are shorter or longer than this optimum value: short molecules spread evenly through the bilayer, while long molecules swell the thicker domain, increasing the surface area and curvature of the bilayer core in the interfacial region. Our results show that adding an appropriate oil could make the formation of domain boundaries more or less favourable, raising the possibility of controlling the domain size distribution.

1 Introduction

Bilayer membranes formed of a mixture of amphiphiles in solution can segregate into domains of different compositions [1]. Research in this area has been driven by two major factors: the suggested role of lipid domains in protein sorting in cell membranes [2] and the capability of domain formation to control the surface properties of a vesicle and to localise not only proteins [3–5] but also enzymes and particles [1] within its wall. Although membrane bilayer domains have been most thoroughly investigated in lipid systems, recent work has moved on to study mixtures of lipids and polymers [6–8], opening up the possibility of more detailed control over bilayer properties such as stiffness, thickness and hydrophobicity [6], and reinforcing the status of membrane domains as an active and important field of research.

The two different types of domain that form in a binary amphiphile mixture may be in the liquid and gel phases respectively [9–12], or may both be in the liquid phase [12–15], albeit with different degrees of internal order in the amphiphile chains [4,12]. Domain formation can be controlled by a variety of factors, including the difference in chain length between the two amphiphile species [4,9,16,17], the lateral tension in the bilayer [11,18] and the presence of a third species, such as a protein or peptide [1,19–22], cholesterol [4,10,12,20], ionised calcium [23] or a ceramide [24].

In this paper, we focus on a system in which two of these factors interact, and use a coarse-grained mean-field model to investigate how adding oil to a bilayer composed of two amphiphiles of different chain lengths affects the structure of the membrane around the boundary between two liquid domains. We have two main reasons for choosing this problem, which also builds on our earlier work on oil droplets in bilayers composed of a single amphiphile species [25]. First, from a practical point of view, we wish to find whether adding oil could prove to be a viable technique for controlling domain formation and the properties of the bilayer. Our second motivation is more theoretical. By choosing two amphiphiles that differ only in length and an oil that is equally compatible with both, we obtain a particularly simple system in which to study the addition of a third species and its effect on bilayer conformation.

More specifically, we aim to find whether varying the size of the added oil molecules can control the inhomogeneity that arises in the membrane surface in the border region [26,27] and its associated free-energy penalties. These determine how favourable the formation of domain boundaries is, which in turn controls the size distribution of domains [26]: if the free-energy cost of forming a domain boundary is high, small domains will tend to fuse together to form larger domains. We will quantify the inhomogeneity at the domain boundary by calculating the changes in the surface area and curvature of the hydrophobic bilayer core induced by changing the size of the oil molecules.

The paper is organised as follows. In the next section, we introduce the coarse-grained mean-field technique to be used,

[a] Institut Charles Sadron, 23, rue du Loess, 67034 Strasbourg, France
[b] Department of Mathematics and Physics, Aberystwyth University, Physical Sciences Building, Aberystwyth, Ceredigion, SY23 3BZ, Wales, UK

self-consistent field theory (SCFT). We then present and discuss the results of our calculations, and give our conclusions in the last section.

2 Self-consistent field theory

Self-consistent field theory (SCFT)[28] has been used over a number of years to model the equilibrium morphologies formed in polymer melts and blends[29–31]. It may also be extended to study metastable structures[32,33] and amphiphiles in solution[34], and has been applied to a wide range of polymers, including homopolymers[35], copolymers[36,37] and mixtures of these[38]. As a mean-field model, SCFT requires less computer time than simulation methods such as Monte Carlo, yet often yields predictions of the form of individual structures that approach these more demanding methods in accuracy[34,39,40]. Furthermore, its simple, coarse-grained description of the polymer molecules will allow us to capture the basic phenomenology of the system clearly.

We now give a short introduction to SCFT, and refer the interested reader to reviews[31,41,42] for an in-depth presentation. A full description of our calculations for amphiphiles in solution is presented in an earlier paper[43], and we give details only when the current system differs from that described there. In SCFT, individual molecules are modelled as random walks in space, with the result that fine details of their packing and structure are not taken into account[42]. An ensemble of many of these molecules is considered, and the inter-molecular interactions are modelled by introducing contact potentials between the molecules and assuming that the blend is incompressible[31]. The strength of the repulsion between the hydrophilic and hydrophobic species is specified by the Flory parameter χ[44]. In order to reduce the computational difficulty of the problem, a mean-field approximation is then made[31]; that is, fluctuations are neglected. In the case of long molecules, this approximation is quantitatively accurate[31,34,41]. Furthermore, SCFT can provide useful qualitative insights when applied to systems containing smaller molecules, particularly lipid bilayers[33] and aqueous solutions of copolymer[45].

We now introduce the implementation of SCFT to our system of two amphiphiles and oil in a solvent, which we model by a mixture of two block copolymers with two incompatible homopolymers that represent the oil and the solvent respectively. Although using a mixture of polymers to represent a amphiphile-solvent system appears slightly simplistic, models of this type have been used to capture the broad phenomenology of a range of lipid and copolymer systems[33,45]. The mean-squared end-to-end distance of the shorter copolymer is set to be a^2N, with a being the monomer length and N the degree of polymerisation[31]. One half of the monomers in this polymer are hydrophilic (type A) and the other half are hydrophobic (type B), so that the degrees of polymerization for the A and B blocks are equal and $N_\mathrm{A} = N_\mathrm{B}$. For simplicity[33], we also set the mean-squared end-to-end distance of the A homopolymer solvent to a^2N. Since we wish to focus on the effect of added oil on the structure of the bilayer, we use a very long second copolymer, with $N_2 \equiv \alpha N = 16N$, so that the inhomogeneity of the bilayer core becomes pronounced around the domain boundary and can be easily studied. We will consider a wide range of oil sizes, and the degree of polymerization $N_\mathrm{O} \equiv \omega N$ of the oil will be varied between $N/8$ and $4N$. Our focus on bilayer structure and geometry also leads us to use oil molecules that are composed of the same material as the hydrophobic B blocks, so that the only interaction parameter χ in the system is that specifying the strength of the repulsion between the A and B species.

In this paper, we fix the amounts of copolymer and homopolymer in the simulation box; that is, we use the canonical ensemble. This will make it easier for us to access more complex structures such as segregated bilayers. Such structures are more difficult to stabilise in ensembles where the system is able to relax by varying the concentrations of the various species, and can require geometric constraints to be applied to the density profile[33].

For completeness and to introduce the notation required for the presentation of our results, we note that the SCFT approximation to the free energy of our system is given by

$$\begin{aligned}\frac{FN}{k_\mathrm{B}T\rho_0 V} &= \frac{F_\mathrm{h}N}{k_\mathrm{B}T\rho_0 V} \\ &- (1/V)\int \mathrm{d}\mathbf{r}\,[\chi N(\phi_\mathrm{A}(\mathbf{r})+\phi_\mathrm{A2}(\mathbf{r})+\phi_\mathrm{S}(\mathbf{r})-\overline{\phi}_\mathrm{A}-\overline{\phi}_\mathrm{A2}-\overline{\phi}_\mathrm{S}) \\ &\times(\phi_\mathrm{B}(\mathbf{r})+\phi_\mathrm{B2}(\mathbf{r})+\phi_\mathrm{O}(\mathbf{r})-\overline{\phi}_\mathrm{B}-\overline{\phi}_\mathrm{B2}-\overline{\phi}_\mathrm{O})] \\ &- (\overline{\phi}_\mathrm{A}+\overline{\phi}_\mathrm{B})\ln(Q_\mathrm{AB}/V) - ((\overline{\phi}_\mathrm{A2}+\overline{\phi}_\mathrm{B2})/\alpha)\ln(Q_\mathrm{AB2}/V) \\ &- \overline{\phi}_\mathrm{S}\ln(Q_\mathrm{S}/V) - (\overline{\phi}_\mathrm{O}/\omega)\ln(Q_\mathrm{O}/V) \qquad (1)\end{aligned}$$

where the $\overline{\phi}_i$ are the mean volume fractions of the different components and the $\phi_i(\mathbf{r})$ are the local volume fractions. For the hydrophilic and hydrophobic blocks of the shorter amphiphile, $i = \mathrm{A}$ and $i = \mathrm{B}$ respectively, and for the corresponding blocks of the longer amphiphile, $i = \mathrm{A2}$ and $i = \mathrm{B2}$. In the cases of the oil and the solvent, $i = \mathrm{O}$ and $i = \mathrm{S}$ respectively. The Flory parameter, χ, is set to $15/N$, as using much larger values than this in conjunction with the long species 2 copolymers could cause numerical instability. V is the total system volume, $1/\rho_0$ is the monomer volume, and F_h is the SCFT free energy of a homogeneous system containing the same components. The details of the individual polymers are contained in the single-chain partition functions Q_i. These are computed[31] by integrating over the propagators q and $q^\dagger$, which are also used to calculate the polymer density profiles[31,41]. Due to the fact that the molecules are modelled as random walks, the propagators are calculated by solving modified diffusion equations with a field term that describes the polymer interactions.

These equations are solved in Cartesian coordinates by a finite difference method[46] with a step size of $0.04aN^{1/2}$. The dimensionless curve parameter s that specifies the distance along the polymer backbone is taken to run from 0 to 1, and its step size in our finite difference method is set to $1/1600$ for the long amphiphile species and $1/400$ for the other species. We assume that the system is translationally invariant along the z-axis, and so consider an effectively two-dimensional problem in a rectangular calculation box. The x-axis is taken to be perpendicular to the domain boundary, and x runs from $-L_x$ to $+L_x$, giving a box length of $2L_x$. Similarly, the y-coordinate takes values from $-L_y$ to L_y. In all calculations presented here, we set $L_x = 14aN^{1/2}$ and $L_y = 4aN^{1/2}$, and impose reflecting boundary conditions at all edges of the system.

The derivation of the mean-field free energy F also generates a set of simultaneous equations relating the fields $w_i(\mathbf{r})$ and densities $\phi_i(\mathbf{r})$. To calculate the SCFT density profiles for a given set of mean volume fractions $\overline{\phi}_i$, we make an initial guess for the fields and solve the diffusion equations to calculate the propagators and then the density profiles corresponding to these fields. The new $\phi_i(\mathbf{r})$ are then substituted into the simultaneous equations to calculate new values for the w_i[47], which are then used in turn to calculate updated values for the ϕ_i by solving the diffusion equation as described above. In order for the algorithm to remain stable, the iteration must be damped, and we do not use these new values of w_i directly to calculate the ϕ_i, but rather the linear combination $\lambda w_i^{\mathrm{new}} + (1-\lambda) w_i^{\mathrm{old}}$ where $\lambda \approx 0.04$. The procedure is repeated until convergence is achieved.

The algorithm can be substantially accelerated by a simple extrapolation procedure. This was developed by observing the typical form of the error in the solution to the SCFT simultaneous equations[31] during the course of the iterations. To begin, we note that, with a suitable initial guess for the fields (such as a broad potential well in $w_{\mathrm{B}}(\mathbf{r})$ for $x < 0$ and a narrow one for $x > 0$), the algorithm converges rapidly to a set of density profiles with the general form of the segregated bilayer we wish to study. However, the SCFT equations are not yet solved, and display a sharp peak in their error terms at the boundary between the two domains. The reason for this is that, although the density profiles have the right overall form, the domain boundary has not yet been correctly located. As the iterations are continued, the x-coordinate of the boundary evolves towards its final value, and the error term peak follows it, gradually decreasing in magnitude. In fact, the magnitude of the error term peak proves to be approximately proportional to the distance of the boundary from its final position along the x-axis. This allows us to perform a simple linear extrapolation to estimate the final value of the domain boundary. We then shift the fields w_i along the x-axis by a distance equal to the difference between the current and predicted boundary positions. These shifted fields will then be used to continue the iterations; however, we first need to deal with two technical issues. First, we note that shifting the fields produces a region at one side of the system where the w_i are not known. Since the shift along the x-axis is relatively small, we simply fill in the unknown region with the values of the w_i at the appropriate end of the unshifted system, $w_i(\pm L_x, y)$. The shift will also have affected the normalisation of the fields, which are usually defined[31] such that $\int \mathrm{d}\mathbf{r}\, w_i(\mathbf{r}) = 0$. Appropriate constants are calculated and added to the fields to correct this problem. This extrapolation procedure need only be used once or twice during the course of the iterations, and can reduce the error term rapidly. We have also used this method to accelerate the convergence of SCFT calculations on large vesicles[48], and it should generalise to a range of density-functional problems involving an interface.

3 Results and discussion

In this section, we investigate the structure of the segregated bilayer for a range of oil molecule sizes by studying the density profiles of the various species. We then look in more detail at the surface of the hydrophobic core of the membrane, and, in particular, at how its area and curvature change as the size of the oil molecules is varied. Finally, we study the effect on the shape and stability of the bilayer of varying the oil concentration. To begin, we calculate the density profiles of segregated bilayers in a system with volume fractions $\overline{\phi}_{\mathrm{A}} + \overline{\phi}_{\mathrm{B}} = 0.06942$, $\overline{\phi}_{\mathrm{A2}} + \overline{\phi}_{\mathrm{B2}} = 0.07246$ and $\overline{\phi}_{\mathrm{O}} = 0.02036$. These values are chosen as they allow the formation of two domains of approximately equal size. They will be kept constant in the first part of our study, although the length of the oil molecules will be varied.

In Figure 1, we plot cuts through the density profiles along the x-axis at $y = 0$. These run through the core of the membrane perpendicular to the interface between the two domains. The first point to note from Figure 1 is simply that solutions do indeed exist to SCFT with the form of segregated bilayers with two clear domains separated by an interface. The domain containing mostly longer amphiphiles is on the left of the interface, and that containing mostly shorter amphiphiles is on the right. The distribution of the oil molecules in the bilayer core depends strongly on their size. In Figure 1a, the oil molecules are much shorter than either of the two amphiphile species, with $\omega = 0.125$. In consequence, they have no strong preference for mixing with one amphiphile or the other, and spread evenly through the two domains. In contrast, the oil molecules used in Figure 1b are longer, with $\omega = 1$, and are the same size as the shorter of the two amphiphiles. This means that they contain twice the number of monomers as the hydrophobic sections of the shorter amphiphiles, and mix less well with the right-hand side of the bilayer. As a result, they are pushed over to the domain formed predominantly of longer molecules,

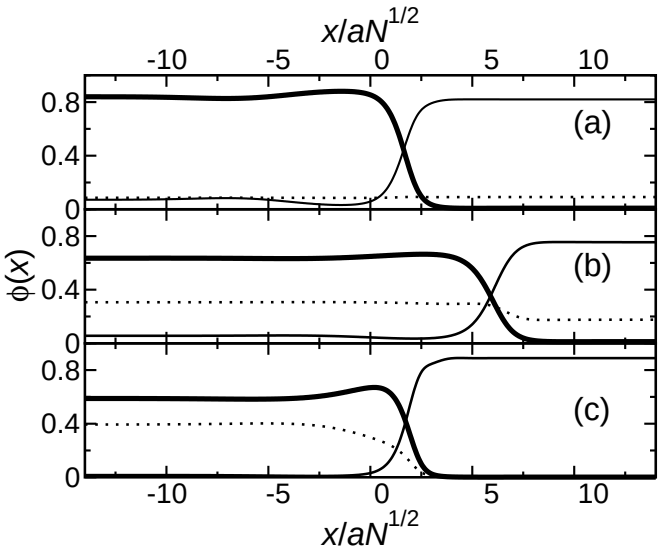

Fig. 1 Cuts through the density profiles in the bilayer core at $y = 0$ for (a) $\omega = 0.125$, (b) $\omega = 1$ and (c) $\omega = 4$. Thick full lines show the local volume fraction of the hydrophobic blocks of the larger amphiphile, thin full lines show the corresponding quantity for the shorter amphiphile, and dotted lines show the local volume fraction of the oil. The concentrations of the hydrophilic blocks are very low in the bilayer core and are omitted for clarity.

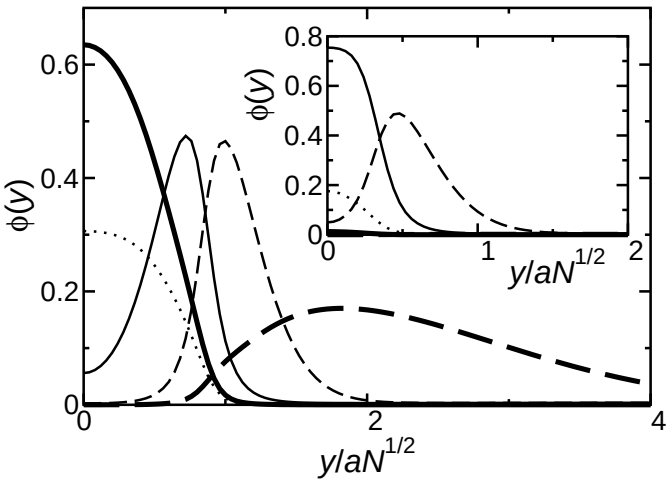

Fig. 2 Cuts through the density profiles at $x = -L_x$ (main panel) and $x = +L_x$ (inset). Thick and thin dashed lines show the local volume fractions of the hydrophilic components of the long and short amphiphiles respectively, and the other species are labelled as in Figure 1.

which swells, moving the domain boundary to the right. We note also that the concentration of oil molecules in both regions is higher in Figure 1b than in Figure 1a. This is because the longer oil molecules have a stronger repulsive interaction with the solvent, as increasing ω increases the product χN, which determines the interaction strength[44]. In Figure 1c, the oil molecules are still longer, with $\omega = 4$, and mix hardly at all with the shorter amphiphiles. However, the swelling of the domain perpendicular to the domain boundary seen in Figure 1b is absent, and the interface has returned to a position close to the centre of the system, as in Figure 1a. A natural explanation for this is that the left-hand side of the bilayer has swollen perpendicular to the plane of the membrane; that is, it has become thicker. We will discuss this point in more detail later.

To give some more insight into the membrane structure, we plot cuts through the density profiles of the various species in the bilayer at the left- and right-hand sides of the system ($x = \pm L_x$) in the direction (y) perpendicular to the plane of the membrane. We focus on the case where $\omega = 1$, the system shown in Figure 1b. In the main panel of Figure 2, we show the density profiles on the left of the system ($x = -L_x$), where the bilayer is formed predominantly of the longer amphiphile species. We see that the structure of the bilayer is more complex than might at first have been expected. Although the core of the membrane is indeed composed mainly of the longer amphiphile species, there is a thinner layer of the shorter amphiphile on the outside of the bilayer, at $y \approx aN^{1/2}$. At the other side of the bilayer ($x = +L_x$), shown in the inset, the structure is simpler, and the bilayer is formed almost exclusively of the shorter species. This shows that the segregation of amphiphiles due only to a difference in size between the two molecular species is far from perfect, with the bilayer formed of the shorter amphiphiles splitting into two leaflets at the domain boundary and coating the outer surface of the thicker domain.

We now proceed to study the effect of the oil molecular size on the structure of the bilayer core in more detail. To this end, we plot the interface between the hydrophobic core and its hydrophilic surroundings, defined as the locus of the points where $\phi_B(x,y) + \phi_{B2}(x,y) + \phi_O(x,y) = 0.5$. For clarity, and to help our later analysis of the bilayer shape, which will involve the calculation of derivatives of the core outline, we fit our discrete SCFT results with a curve of the form

$$y(x) = a_0 + \frac{a_1}{1+\exp[-(x-a_2)/a_3]} + a_4 \exp[-(x-a_5)^2/a_6] \quad (2)$$

where the a_i are adjustable parameters. This formula gives an excellent fit to the data.

These results are shown in Figure 3. The dotted line shows the outline of the membrane core when the oil molecules are very short, with $\omega = 0.125$. Here, the core profile has a noticeable lip region on the left-hand side of the bilayer just before the domain boundary, which is located close to the centre of the system. As the size of the oil molecules is increased, so that $\omega = 1$, they are pushed into the thicker side of the bilayer,

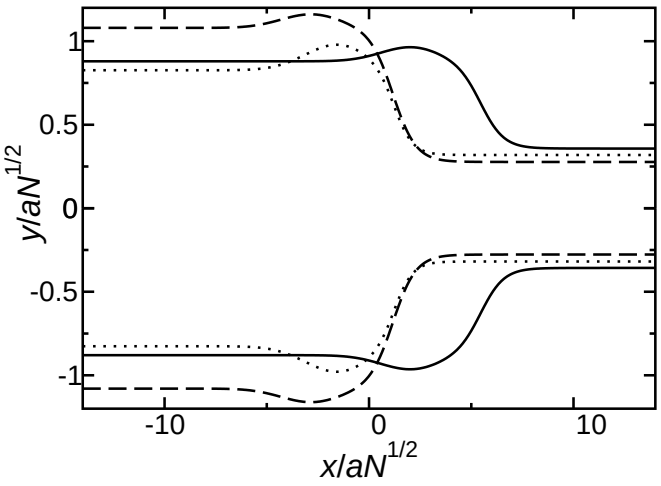

Fig. 3 Outlines of the hydrophobic bilayer core for $\omega = 0.125$ (dotted lines), $\omega = 1$ (full lines) and $\omega = 4$ (dashed lines). Note the difference in scale between the x and y axes.

as already seen in Figure 1b. We then obtain the core profile plotted with a full line in Figure 3, where the area of the left-hand domain has increased and the domain boundary has moved to the right.

The plots of the core outlines now bring out some features of this phenomenon that were not apparent from the cuts through the density profiles shown in Figure 1. First, we see that the thickness of the left domain increases relatively little as ω is increased from 0.125 to 1. This is because, although the oil molecules are now longer than the hydrophobic components of the shorter amphiphiles and can no longer easily be accommodated on the right-hand side of the bilayer, they are still sufficiently short to mix well with the corresponding sections of the larger amphiphiles without causing the left-hand side of the bilayer to thicken. The left domain then accommodates the extra oil by increasing its area rather than its thickness, leading to the shift of the domain boundary to the right noted earlier. In addition, we see that this has the effect of smoothing the surface of the bilayer core, reducing the size of the lip feature just before the domain boundary, and also reducing the slope of the core profile $y(x)$ at the boundary itself.

As ω is increased still further, to a value of 4, we obtain the core profile plotted with a dashed line in Figure 3. In this case, the oil molecules are almost all located on the left. Furthermore, their length means that they now increase the thickness of the left-hand domain. This means that it is now no longer necessary for this domain to grow in area in order to accommodate the oil molecules, and the interface is again found close the centre of the system.

In our discussion of the bilayer core outlines plotted in Figure 3, we noted several effects of varying the size of the oil molecules: changes in the bilayer thicknesses, the domain sizes and the structure of the interfacial region. We now wish to proceed to a more quantitative analysis of the core shape. First, by comparing the core outlines for $\omega = 0.125$ and $\omega = 4$ (dotted and dashed lines respectively), we see that the significant difference in the left-hand domain thickness between the two bilayers leads to a larger surface area of the bilayer core when $\omega = 4$, visible as an increase in the length of the outline plotted in Figure 3. This increases the contact between the hydrophobic core and the solvent, leading to a sharp increase in the free energy[49]. To quantify the differences in core surface area between the different bilayers, we calculate the excess area

$$\Delta A = \int \mathrm{d}x \left[\sqrt{1 + (\mathrm{d}y(x)/\mathrm{d}x)^2} - 1 \right] \qquad (3)$$

in each case, using the fits to our SCFT data given by Equation 2, and plot the results as a function of ω in Figure 4a. Since the two bilayer domains are flat, the major contributions to ΔA come from the boundary region. Calculating ΔA will therefore give us insight into the free-energy penalty incurred by the introduction of a domain boundary into the system.

From Figure 4a, we see at once that the excess surface area ΔA has a clear minimum at $\omega \sim 1$. This is a result of two of the effects discussed above. The transfer of oil to the left domain as ω is increased initially leads to a lateral expansion of this region and a smoothing of the lip feature, resulting in a fall in ΔA. However, as ω is increased further, the difference in thickness between the two domains grows, causing an increase in ΔA. These results show that there is an optimum oil size at which the free energy penalty arising from the excess surface area can be minimised in our system.

The lowest free-energy state of a symmetric bilayer is flat, and deviations from this shape will lead to an increase in its free energy[50]. These deviations can be characterised by the curvatures of the membrane leaflets. Although our laterally segregated membrane is more complex than a bilayer vesicle or a monolayer of surfactants at an oil-water interface, situations which can be studied in detail by models based wholly on membrane curvature[50], study of its surface curvature should still give insight into how the addition of oil molecules of various sizes pushes the bilayer into more or less favourable configurations. Since the core outlines have the form $y = y(x)$, we can calculate the squared curvature integrated over the bilayer from $x = -L_x$ to $x = +L_x$ using

$$K^2 = \int_{-L_x}^{+L_x} \mathrm{d}x \frac{(\mathrm{d}^2 y(x)/\mathrm{d}x^2)^2}{[1 + (\mathrm{d}y(x)/\mathrm{d}x)^2]^3} \qquad (4)$$

In Figure 4b, we plot K^2 as a function of oil size. As in the case of the excess surface area, we see a clear minimum around $\omega \sim 1$, where the oil molecules move into the thicker bilayer domain and smooth the surface. The form of the curve is slightly different than that seen for ΔA, with K^2 increasing

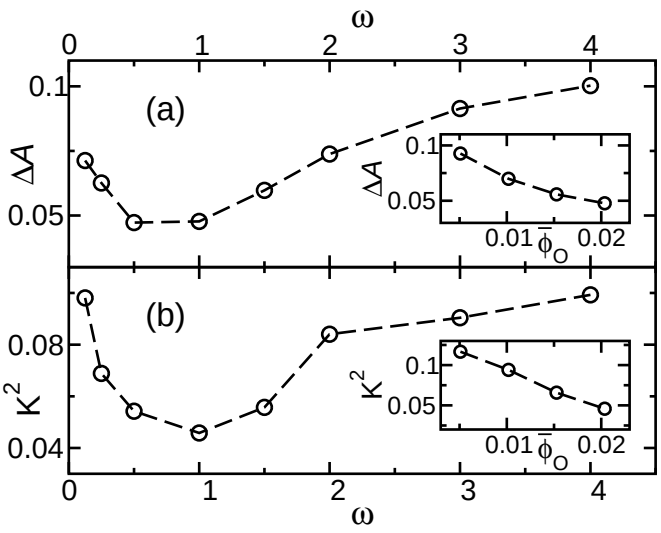

Fig. 4 (a) Excess surface area of the hydrophobic bilayer core plotted as a function of oil size. Inset shows excess surface area plotted against oil concentration for $\omega = 1$. (b) Corresponding plots of the integrated squared curvature of the hydrophobic bilayer core.

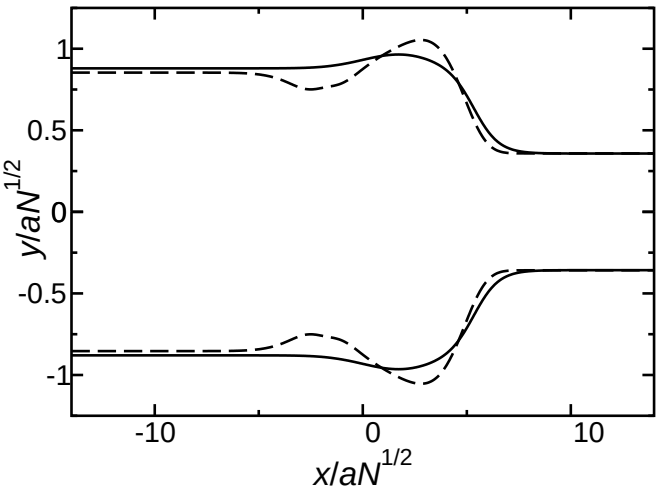

Fig. 5 Outlines of the hydrophobic bilayer core for $\overline{\phi}_{\rm O} = 0.00509$ (dashed lines), and $\overline{\phi}_{\rm O} = 0.02036$ (full lines).

rapidly between $\omega = 1$ and $\omega = 2$ before levelling off somewhat for $\omega > 2$. The reason for this is that, although the growth in the difference in thickness between the two domains for $\omega > 2$ requires an increase in the surface area of the bilayer core in the domain boundary region, it does not need a similar increase in its curvature, since the new surface area in the step region is close to being flat. This can be seen by looking at the dashed outline ($\omega = 4$) in Figure 3 and comparing it with the other two outlines.

Finally, we examine the effect of lowering the oil concentration $\overline{\phi}_{\rm O}$ on the bilayer shape. In the following calculations, when we reduce $\overline{\phi}_{\rm O}$ by a given amount, we increase each of the concentrations $\overline{\phi}_{\rm AB}$ and $\overline{\phi}_{\rm AB2}$ by the same amount. This keeps the total amount of hydrophobic B material in the system constant, since both the amphiphile species contain equal amounts of hydrophilic and hydrophobic monomers. The insets to Figure 4a and b show the effect of this on ΔA and K^2 respectively for the case of $\omega = 1$. Both quantities rise appreciably as the oil concentration falls. ΔA increases by a factor of two as $\overline{\phi}_{\rm O}$ is decreased by a factor of four, and K^2 rises still more, reaching higher values than were obtained for the original oil concentration even for $\omega = 4$.

These increases reflect a change in the bilayer shape: the lip feature near the domain boundary has become more pronounced. In fact, to calculate ΔA and K^2 for the lowest oil concentration shown in the insets to Figure 4, we need to add an extra term to Equation 2 in order to account for the increased inhomogeneity in the surface of the bilayer core. We find a fit of the same high quality as before is obtained if this term takes the form $a_7 \exp[-(x-a_8)^4/a_9]$, where the a_i are adjustable coefficients. The outline of the bilayer core for the lowest oil concentration considered, $\overline{\phi}_{\rm O} = 0.00509$, one quarter of the original value, is plotted with a dashed line in Figure 5. The corresponding outline at the original $\overline{\phi}_{\rm O}$ is shown for reference, and the difference in the surface structure between the two bilayers is clear.

The inhomogeneity of the bilayer in the junction region observed in Figure 5 reflects an increasing instability in the bilayer structure. If we set the oil concentration to zero and increase the amphiphile concentrations so that the total amount of hydrophobic material remains constant, as described before, the segregated bilayer structure is no longer stable, and splits into separate thick and thin bilayers. This shows that, in our system, the oil is a necessary stabilising factor to overcome the strong size mismatch between the two amphiphile species.

4 Conclusions

Using a coarse-grained mean-field model, we have investigated the effect of added oil on the structure of the boundary between two domains in a segregated bilayer formed of a mixture of long and short amphiphiles. We have found that adding oil molecules is a promising method for controlling the inhomogeneity of the bilayer core surface in the vicinity of the domain boundary. In particular, we have shown that, in our model, the surface area of the hydrophobic core exposed to the solvent and the curvature of the hydrophobic-hydrophilic interface depend in a very similar way on the length of the oil molecules, and could therefore be adjusted simultaneously to tune the free energy associated with boundary formation and

hence the size distribution of the domains. The existence of an optimum chain length at which the surface free-energy penalties are minimised can be viewed as an example of a *cut-off effect*[51,52]. In a number of situations in biology, such as anaesthesia[51], the influence of a long-chain molecule added to a system increases with increasing chain length n before falling off above a certain critical value. This effect is reviewed in detail by Balgavý and Devínsky[51], who also anticipate the current work[51,53] by suggesting that the distribution of an added species in a bilayer composed of a mixture of different lipids could control its biological properties. Our last finding is that bilayers with added oil are found to be stable even when a large difference in size between the two amphiphiles leads the corresponding oil-free bilayer to split.

We now discuss possible extensions to our work that could reinforce and add detail to our conclusions. First, we reiterate that the curvature and, particularly, the surface area of the hydrophobic core in the domain boundary region will be two important factors in determining the free energy of the boundary, or line tension. In fact, the energy cost in changing the surface area of a membrane is so high that bilayer vesicles have an almost constant area at constant temperature[49]. Any procedure that alters the membrane surface area at the boundary between two domains therefore has clear potential for controlling the line tension. However, it would be helpful to back this up by carrying out a more detailed study of the thermodynamics of the membrane. For instance, the line tension could be separated out directly from the SCFT free energy of our system by subtracting the energy of the two domains with a step boundary. At present, this calculation is difficult, as the calculated numerical value for the line tension is small in comparison to the other contributions to the free energy, such as that arising from the aggregation of the large amphiphiles into a bilayer. A more detailed investigation, perhaps involving calculations performed on a finer grid and a study of finite-size effects, would be necessary for us to have full confidence in our calculation of this quantity. The lateral tension in the bilayer could also be investigated in more detail, as it too will be affected by the changes in surface area introduced by the oil. For example, a decrease in surface area could lead to an increase in the lateral tension. The thermodynamic ensemble could also be chosen to perform the calculations at constant lateral tension rather than constant area.

At present, the size mismatch between the two amphiphiles in our system is very large. This was a deliberate choice in order to bring out the effects of oil on the bilayer shape as clearly as possible. However, the size difference in a real system will be smaller, and it would be very useful to extend our calculations to a more realistic size ratio. Our assumption of zero repulsive interactions between the two amphiphile species could also be relaxed, to allow for a degree of chemical incompatibility. These calculations could involve more detailed modelling of the amphiphiles and oil, perhaps involving extensions of SCFT beyond the Gaussian chain approximation[54], allowing us to be more specific about the chemical nature of the molecules involved.

5 Acknowledgements

M.J.G. gratefully acknowledges funding from the EU under an FP7 Marie Curie fellowship and from the IRTG Soft Matter Science.

References

1 L. A. Bagatolli, J. H. Ipsen, A. C. Simonsen and O. G. Mouritsen, *Prog. Lipid Res.*, 2010, **49**, 378–389.
2 D. A. Brown and E. London, *Annu. Rev. Cell Dev. Bi.*, 1998, **14**, 111–136.
3 F. Dumas, M. M. Sperotto, M.-C. Lebrun, J.-F. Tocanne and O. G. Mouritsen, *Biophys. J.*, 1997, **73**, 1940–1953.
4 J. Domański, S. J. Marrink and L. V. Schäfer, *Biochim. Biophys. Acta*, 2012, **1818**, 984–994.
5 Z. Salamon, S. Devanathan, I. D. Alves and G. Tollin, *J. Biol. Chem.*, 2005, **280**, 11175–11184.
6 M. Schulz, D. Glatte, A. Meister, P. Scholtysek, A. Kerth, A. Blume, K. Bacia and W. H. Binder, *Soft Matter*, 2011, **7**, 8100–8110.
7 P. C. Seitz, M. Reif, K. Yoshikawa, R. Jordan and M. Tanaka, *J. Phys. Chem. B*, 2011, **115**, 2256–2263.
8 T. Ruysschaert, A. F. P. Sonnen, T. Haefele, W. Meier, M. Winterhaltet and D. Fournier, *J. Am. Chem. Soc.*, 2005, **127**, 6242–6247.
9 R. Faller and S. J. Marrink, *Langmuir*, 2004, **20**, 7686–7693.
10 P. W. Tumaneng, S. A. Pandit, G. Zhao and H. L. Scott, *Phys. Rev. E*, 2011, **83**, 031925.
11 T. Hamada, Y. Kishimoto, T. Nagasaki and M. Takagi, *Soft Matter*, 2011, **7**, 9061–9068.
12 J. Zhao, J. Wu, F. A. Heberle, T. T. Mills, P. Klawitter, G. Huang, G. Costanza and G. W. Feigenson, *Biochim. Biophys. Acta*, 2007, **1768**, 2764–2776.
13 S. H.-W. Wu and H. M. McConnell, *Biochemistry*, 1975, **14**, 847–854.
14 S. L. Veatch, I. V. Polozov, K. Gawrisch and S. L. Keller, *Biophys. J.*, 2004, **86**, 2910–2922.
15 P. Garidel, C. Johann and A. Blume, *Biophys. J.*, 1997, **72**, 2196–2210.
16 J. Risbo, M. M. Sperotto and O. G. Mouritsen, *J. Chem. Phys.*, 1995, **103**, 3643–3656.
17 J. Sanchez and A. Badia, *Thin Solid Films*, 2003, **440**, 223–239.
18 S. A. Akimov, P. I. Kuzmin, J. Zimmerberg and F. S. Cohen, *Phys. Rev. E*, 2007, **75**, 011919.
19 S. A. Akimov, V. A. J. Frolov, P. I. Kuzmin, J. Zimmerberg, Y. A. Chizmadzhev and F. S. Cohen, *Phys. Rev. E*, 2008, **77**, 051901.
20 S. Janosch, C. Nicolini, B. Ludolph, C. Peters, M. Völkert, T. L. Hazlet, E. Gratton, H. Waldmann and R. Winter, *J. Am. Chem. Soc.*, 2004, **126**, 7496–7503.
21 M. M. Sperotto and O. G. Mouritsen, *Eur. Biophys. J.*, 1993, **22**, 323–328.
22 H. Jing, H. Kim, D. Choi, D. R. Lee, J. S. Lee, C.-J. Yu and K. Shin, *Biointerphases*, 2011, **6**, 73–78.
23 W. Knoll, H.-J. Apell, H. Eibl and A. Miller, *Eur. Biophys. J.*, 1986, **13**, 187–193.
24 B. Westerlund, P.-M. Grandell, Y. J. E. Isaksson and J. P. Slotte, *Eur. Biophys. J.*, 2010, **39**, 1117–1128.
25 M. J. Greenall and C. M. Marques, *Soft Matter*, 2012, **8**, 3308–3314.

26 S. A. Akimov, P. I. Kuzmin, J. Zimmerberg, F. S. Cohen and Y. A. Chizmadzhev, *J. Electroanal. Chem.*, 2004, **564**, 13–18.

27 P. I. Kuzmin, S. A. Akimov, Y. A. Chizmadzhev, J. Zimmerberg and F. S. Cohen, *Biophys. J.*, 2005, **88**, 1120–1133.

28 S. F. Edwards, *Proc. Phys. Soc.*, 1965, **85**, 613–624.

29 P. Maniadis, T. Lookman, E. M. Kober and K. O. Rasmussen, *Phys. Rev. Lett.*, 2007, **99**, 048302.

30 F. Drolet and G. H. Fredrickson, *Phys. Rev. Lett.*, 1999, **83**, 4317–4320.

31 M. W. Matsen, in *Soft Matter*, Wiley-VCH, Weinheim, 2006, ch. 2.

32 D. Duque, *J. Chem. Phys.*, 2003, **119**, 5701–5704.

33 K. Katsov, M. Müller and M. Schick, *Biophys. J.*, 2004, **87**, 3277–3290.

34 A. Cavallo, M. Müller and K. Binder, *Macromolecules*, 2006, **39**, 9539–9550.

35 A. Werner, M. Müller, F. Schmid and K. Binder, *J. Chem. Phys.*, 1999, **110**, 1221–1229.

36 M. Müller and G. Gompper, *Phys. Rev. E*, 2002, **66**, 041805.

37 J. F. Wang, K. K. Guo, L. J. An, M. Müller and Z. G. Wang, *Macromolecules*, 2010, **43**, 2037–2041.

38 N. A. Denesyuk and G. Gompper, *Macromolecules*, 2006, **39**, 5497–5511.

39 C. M. Wijmans and P. Linse, *Langmuir*, 1995, **11**, 3748–3756.

40 F. A. M. Leermakers and J. M. H. M. Scheutjens, *J. Colloid Interface Sci.*, 1990, **136**, 231–241.

41 G. H. Fredrickson, *The Equilibrium Theory of Inhomogeneous Polymers*, Oxford University Press, Oxford, 2006.

42 F. Schmid, *J. Phys.: Condens. Matter*, 1998, **10**, 8105–8138.

43 M. J. Greenall and G. Gompper, *Langmuir*, 2011, **27**, 3416–3423.

44 R. A. L. Jones, *Soft Condensed Matter*, Oxford University Press, Oxford, 2002.

45 P. Schuetz, M. J. Greenall, J. Bent, S. Furzeland, D. Atkins, M. F. Butler, T. C. B. McLeish and D. M. A. Buzza, *Soft Matter*, 2011, **7**, 749–759.

46 W. H. Press, B. P. Flannery, S. A. Teukolsky and W. T. Vetterling, *Numerical Recipes in C*, Cambridge University Press, Cambridge, 2nd edn, 1992.

47 M. W. Matsen, *J. Chem. Phys.*, 2004, **121**, 1938–1948.

48 M. J. Greenall and C. M. Marques, *Phys. Rev. Lett.*, 2013, **110**, 088301.

49 U. Seifert, *Adv. Phys.*, 1997, **46**, 13–137.

50 S. A. Safran, P. A. Pincus, D. Andelman and F. C. MacKintosh, *Phys. Rev. A*, 1991, **43**, 1071–1078.

51 P. Balgavý and F. Devínsky, *Adv. Colloid Interface Sci.*, 1996, **66**, 23–63.

52 J. M. Pope, L. W. Walker and D. Dubro, *Chem. Phys. Lipids*, 1984, **35**, 259–277.

53 F. Sersen, A. Leitmanová, F. Devínsky, I. Lacko and P. Balgavý, *Gen. Physiol. Biophys.*, 1989, **8**, 133–156.

54 M. W. Matsen, *Macromolecules*, 2012, **45**, 8502–8509.